PHYSICAL REVIEW C **96**, 055209 (2017)

Compton scattering from ^{4}He at 61 MeV

M. H. Sikora,[1,2,*] M. W. Ahmed,[1,2,3] A. Banu,[4] C. Bartram,[2,5] B. Crowe,[2,3] E. J. Downie,[6] G. Feldman,[6] H. Gao,[1,2] H. W. Grießhammer,[6] H. Hao,[2] C. R. Howell,[2] H. J. Karwowski,[2,5] D. P. Kendellen,[1,2] M. A. Kovash,[7] X. Li,[1,2] D. M. Markoff,[2,3] S. Mikhailov,[2] V. Popov,[2] R. E. Pywell,[8] J. A. Silano,[2,5] M. C. Spraker,[9] P. Wallace,[2] H. R. Weller,[1,2] C. S. Whisnant,[4] Y. K. Wu,[1,2] W. Xiong,[1,2] X. Yan,[1,2] and Z. W. Zhao[1,2]

[1]*Department of Physics, Duke University, Durham, North Carolina 27708-0308, USA*
[2]*Triangle Universities Nuclear Laboratory, Durham, North Carolina 27708-0308, USA*
[3]*Department of Mathematics and Physics, North Carolina Central University, Durham, North Carolina, 27707, USA*
[4]*Department of Physics and Astronomy, James Madison University, Harrisonburg, Virginia 22807, USA*
[5]*University of North Carolina at Chapel Hill, Chapel Hill, North Carolina 27516, USA*
[6]*Institute for Nuclear Studies, Department of Physics, The George Washington University, Washington DC 20052, USA*
[7]*Department of Physics & Astronomy, University of Kentucky, Lexington, Kentucky 40508, USA*
[8]*Department of Physics and Engineering Physics, University of Saskatchewan, Saskatoon, Saskatchewan, S7N 5E2, Canada*
[9]*Department of Physics, University of North Georgia, Dahlonega, Georgia 30597, USA*

(Received 22 August 2017; published 27 November 2017)

The Compton scattering cross section from ^{4}He has been measured with high statistical accuracy over a scattering angle range of $40^\circ - 159^\circ$ using a quasimonoenergetic 61-MeV photon beam at the High Intensity Gamma-Ray Source. The data are interpreted using a phenomenological model sensitive to the dipole isoscalar electromagnetic polarizabilities (α_s and β_s) of the nucleon. These data can be fit with the model using values of α_s and β_s that are consistent with the currently accepted values. These data will serve as benchmarks of future calculations from effective field theories and lattice quantum chromodynamics.

DOI: 10.1103/PhysRevC.96.055209

I. INTRODUCTION

Electromagnetic probes are highly efficient, perturbative tools to explore the symmetries and dynamics of the internal structure of nucleons. They test the competition between the electromagnetic force and the strong forces that bind the nucleons. Such information is encoded in the static electric (α_E) and magnetic (β_M) dipole polarizabilities. These fundamental properties parametrize the two-photon response of the nucleon, i.e., the stretchability of the electric charge distribution and the alignability of its magnetic constituents. They are probed by Compton scattering, where the electromagnetic field of a real photon induces radiation multipoles by displacing charges and currents inside the nucleon.

At low energies, effective field theories (EFTs) describe such processes model-independently in terms of the pertinent low-energy degrees of freedom: nucleons and pions. In the past decade, they were used with great success to predict and extract the proton and neutron polarizabilities from Compton scattering data [1,2] and to connect these data with emerging lattice quantum chromodynamics (QCD) calculations; see most recently Refs. [3–13]. Such tests of low-energy QCD rely on the decades-long effort to obtain high-precision data of Compton scattering on the proton and light nuclei; see Ref. [14] for a review.

The proton polarizabilities have been extracted from measurements using cryogenic liquid H_2 targets [15–19], whereas the neutron values have been extracted from elastic (and, to a lesser extent, inelastic) deuteron Compton scattering [20]. Since the electromagnetic fine structure constant is small and enters quadratically, cross sections are relatively small but increase with the target charge Z for light nuclei. In addition, only light nuclei can provide stable targets to extract neutron polarizabilities. Finally, the charged pieces of the pion exchange that contribute to binding the nucleons in nuclei also increase the cross section.

High-precision Compton scattering experiments have recently been performed using targets with $Z > 1$, in particular ^{6}Li [21,22], for future extractions of nucleon polarizabilities using EFTs. Because there are no *ab initio* or EFT calculations at this time, phenomenological models are used to interpret data from Compton scattering from light nuclei [23]. This work reports results of Compton scattering from a liquid ^{4}He target.

Data from ^{4}He complement and improve on that available from deuteron Compton scattering in a number of ways. First, the cross section for Compton scattering from ^{4}He is approximately a factor of 8 larger than the deuteron due to the combination of the larger nuclear charge and charged pion exchange current. Second, both are isoscalar targets, so that one has direct access to the average nucleon polarizability and can infer the less-certain neutron values by combining with the well-established proton values. Third, the weakly bound (2.25 MeV) deuteron requires high energy-resolution measurements to separate the elastic and inelastic contributions to the cross section. However, the first inelastic channel is the ^{4}He$(\gamma, p)^3$H reaction at 19.8 MeV, alleviating the need of a high energy-resolution measurement. Finally, the data will test the accuracy to which theoretical efforts describe binding effects in the deuteron and ^{4}He in a common framework.

This paper presents the first high-precision measurement of the ^{4}He Compton scattering cross section with wide

*msikora@tunl.duke.edu

angular coverage. The measurements were performed using the circularly polarized, monoenergetic γ-ray beam at the High Intensity Gamma-Ray Source (HIγS) facility of the Triangle Universities Nuclear Laboratory (TUNL). Data are interpreted using a previously developed phenomenological model [23].

II. EXPERIMENTAL SETUP

The HIγS facility [24] uses a free electron laser to produce intense, quasimonoenergetic, $\sim$100% polarized γ-ray beams via Compton back-scattering. This process occurs at a frequency of 5.79 MHz, generating γ-ray pulses every 179 ns. These characteristics of the HIγS beam result in scattering spectra that are cleaner and much simpler to interpret compared to Compton scattering experiments conducted with tagged bremsstrahlung beams.

After collimation of the γ-ray beam, its intensity was continuously monitored using a system of five thin plastic scintillator paddles [25] located upstream of the target. Recoil electrons and positrons produced in a thin metal radiator are detected in the paddles at a rate proportional to the incident flux. The system was calibrated using a 100% efficient NaI(Tl) detector to determine the conversion factor between the observed paddle rate and the total number of detected γ rays. This system provides a continuous method of measuring the incident flux. The present experiment utilized a circularly polarized 61-MeV beam with an intensity of $\sim 2 \times 10^7\ \gamma/s$ on target for a total of 54 h.

The liquid ^{4}He target was inside an aluminum vacuum can of diameter 46 cm [26]. The target cell was a Kapton cylinder with 0.13-mm-thick walls and dimensions 20 cm long $\times$ 4 cm diameter. The beam entered and exited the vacuum can through Kapton windows also of 0.13-mm thickness located along the beam axis. The liquid temperature was monitored continuously throughout the experiment to ensure that the target thickness was known to $\sim$1%. The liquid was maintained in the cell at 3.17 K for a target thickness of $(4.22 \pm 0.04) \times 10^{23}$ nuclei/cm^2. Scattering data were also collected with no liquid in the cell to assess the contribution from the windows and cell walls, which was found to be $\sim$15% of the full-target yield in each detector.

Energy spectra were obtained using seven NaI(Tl) detectors positioned at angles ranging from 40° to 159° with the front face of each detector approximately 58 cm from the target center, as illustrated in Fig. 1. The core crystals, measuring 25.4 cm in diameter and ranging in length from 25.4 to 30.5 cm, were surrounded by a 7.5-cm-thick segmented anticoincidence shield consisting of eight NaI(Tl) crystals 30.5 cm in length. The acceptance cone of each core detector was defined by a 15-cm-thick lead collimator, resulting in a Gaussian distribution of scattering angles with a standard deviation of 5°. The detector apertures were filled with borated wax to suppress background neutrons. The experiment was surveyed to a precision of 0.1 cm, and the measurements were incorporated into a GEANT4 [27] simulation. In the simulation, photons were generated throughout the target volume and propagated outward following a spherical angular distribution. The fraction of the emitted photons observed in each detector was proportional to its effective solid angle. The nominal effective solid angle of each detector is 43 msr.

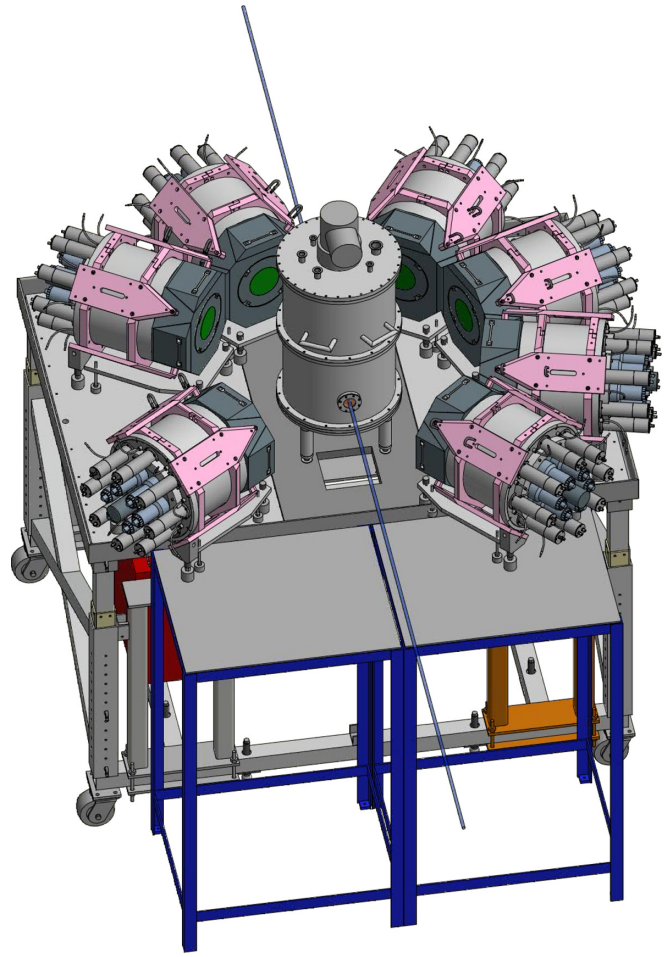

FIG. 1. Illustration of the experimental geometry showing the array of NaI(Tl) detectors and the cryogenic target. The beam is incident from the top of the figure. The Kapton cell containing the liquid ^{4}He is located inside the vacuum can.

III. DATA ANALYSIS

Two analog copies of each core NaI detector signal were generated. One copy from each detector was shaped and amplified using a timing filter amplifier (TFA). Each subsequent TFA output was subjected to an analog threshold using a constant fraction discriminator (CFD). A logical OR of all core detectors was used to produce a trigger for the data acquisition system. This trigger generated a 2-μs acquisition window on a 14-bit, 500 MHz waveform digitizer which recorded the pulse shape of the second copy of the core NaI signal. The signals from the eight individual shield elements associated with each core were combined into a single waveform before being digitized, reducing the required number of digitizer channels. The time difference between an event trigger and a beam-pulse time reference signal from the accelerator was measured with a time-to-amplitude converter (TAC), and the output was then recorded on a dedicated digitizer channel. The detector waveforms were charge-integrated to extract the

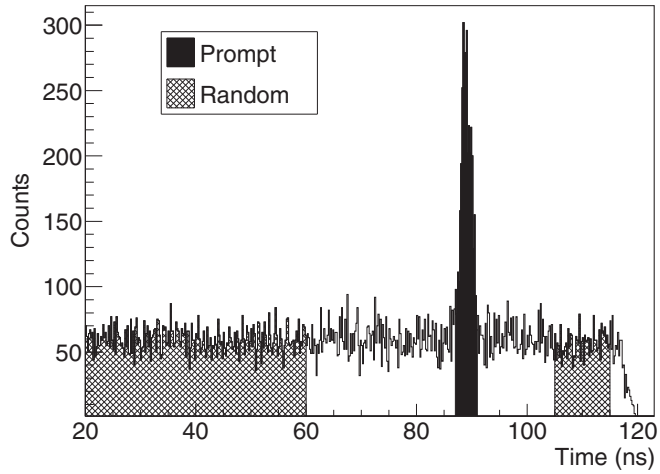

FIG. 2. Timing spectrum after applying the shield cut showing prompt (solid) and random (hatched) regions.

energy deposited in the detector, and the TAC signal was peak-sensed to produce timing spectra for each detector.

The pulsed nature of the HIγS beam yielded a prominent prompt timing peak for events produced from a beam burst, while non-beam-related events have a flat, random timing distribution (Fig. 2). The uncorrelated background, primarily due to high-energy cosmic rays, occurring within the prompt window can be suppressed by considering the energy deposited in the shields. The path of γ rays originating in the target through the core crystals is restricted by the lead collimator in front of each detector to accept only event sites along the beam axis that can fully illuminate the back face of the core without directly intersecting the shield segments. The energy deposited in the shields for scattering events is primarily due to electromagnetic shower losses in the core crystal and is therefore much lower compared to the energy deposited in the shields from high-energy cosmic rays. An analysis using the aforementioned simulation demonstrated that the shield energy deposition can reduce the cosmic-ray background without affecting the acceptance of Compton scattering events from the target. The application of both the timing and shield energy cuts is able to reject 99.9% of the cosmic-ray background over the Compton scattering peak region in the energy spectrum. The remaining time-uncorrelated background was accounted for by taking energy spectra from the randoms region in the γ-ray time-of-flight spectrum shown in Fig. 2 after applying the shield energy cut. The randoms region was chosen so as to exclude fast neutrons from ^{4}He break up, which would appear in the immediate vicinity of the prompt peak. The energy spectrum of events in the randoms region was then scaled by the relative width of the prompt/random time intervals and subtracted from the energy spectrum obtained from the prompt region.

Examples of the resulting energy spectra of the scattered γ rays obtained after applying the above analysis are shown in Fig. 3 for two Compton scattering angles with the target cell full and empty. The empty-target subtracted spectra are shown in Fig. 4 for the same scattering angles along with GEANT4 simulations of the detector response function. After

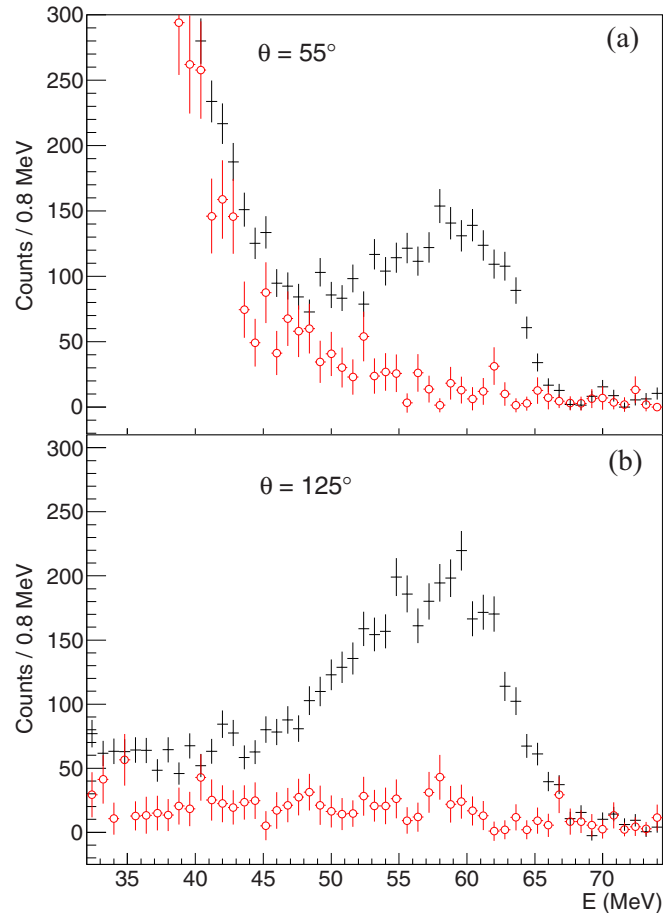

FIG. 3. Comparison of full-target (crosses) and empty-target (open circles) energy spectra. The empty-target data have been normalized to the number of incident photons.

removing the empty-target contribution, the forward-angle spectra contain a low-energy exponential background that is assumed to be due to atomic scattering, which is kinematically suppressed at backward angles. The aforementioned GEANT4 simulation was used to separate this contribution from the scattering spectrum [Fig. 4(a)]. Detector response functions were obtained using the GEANT4 simulation by generating photons uniformly throughout the target volume and recording the energy subsequently deposited in a detector volume. The initial energy of the generated photons E' was calculated based on the outgoing scattering angle θ according to the well-known Compton scattering formula,

$$E' = \frac{E_\gamma}{1 + (E_\gamma / AM_N)(1 - \cos\theta)}, \tag{1}$$

where $E_\gamma = 61$ MeV is the γ-ray beam energy and AM_N denotes the nuclear mass of ^{4}He. The resulting line shape accounts for absorption in the target cell and the vacuum can as well as geometric effects but not for the intrinsic detector resolution and the energy spread of the beam. A Gaussian smearing function was applied to each individual line shape to fit the scattering data, and the forward angle detectors were simultaneously fit with an exponential function. Typical fit

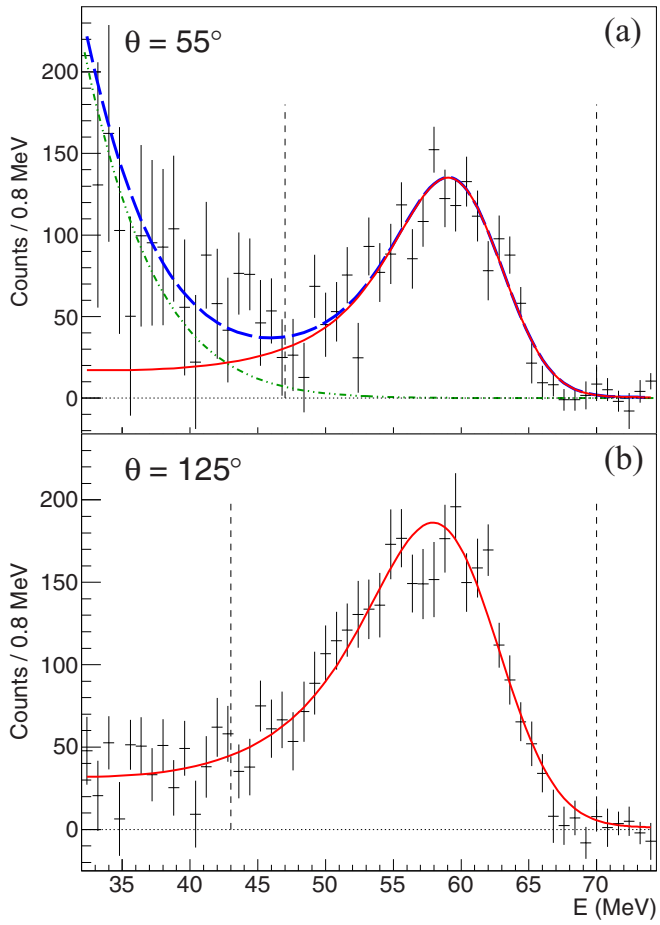

FIG. 4. (a) Energy spectrum at $\theta = 55^\circ$ after removing the empty target contribution. The total response at forward angles (dashed line) includes an exponential low-energy background from atomic processes (dot-dashed line) and a detector response function (solid line) obtained from GEANT4 . (b) Energy spectrum at $\theta = 125^\circ$ after removing the empty target contribution. The backward angle spectra are background-free and are well-described by the simulated detector response (solid line). Yields are extracted from the indicated integration regions.

results are displayed in Fig. 4, along with the integration region (indicated by the vertical dashed lines) used to extract yields. The fraction of the fitted line shape contained within the integration region is calculated and used as an efficiency factor in the evaluation of the cross section. The lowest energy inelastic channel is the two-body ^{4}He$(\gamma,p)^3$H reaction with a threshold energy of 19.8 MeV so that inelastic scattering is not expected to contribute to the yield extracted from the indicated summing regions.

IV. PHENOMENOLOGICAL MODEL

The sensitivity of these data to the isoscalar electromagnetic dipole polarizabilities can be assessed using a phenomenological model based on the total photoabsorption cross section [23]. As described by Feldman *et al.* [28] and discussed for the case of ^{4}He by Führberg *et al.* [29], the Compton scattering amplitude can be written as

$$R(E,\theta) = R^{\rm GR}(E,\theta) + R^{\rm QD}(E,\theta) + R_1^{\rm SG}(E,\theta) + R_2^{\rm SG}(E,\theta), \quad (2)$$

where $R^{\rm GR}$ describes the giant resonance response, $R^{\rm QD}$ is the quasideuteron amplitude, and $R_1^{\rm SG}$ and $R_2^{\rm SG}$ are the one- and two-body seagull (SG) amplitudes, which depend explicitly on the isoscalar electric and magnetic dipole polarizabilities, α_s and β_s.

The $R^{\rm GR}$ and $R^{\rm QD}$ terms are composed of complex forward scattering amplitudes $f_\lambda(E)$ taken to be Lorentzians, which are multiplied by an angular factor $g_\lambda(\theta)$ based on the multipole λ of the transition

$$R^{\rm GR}(E,\theta) = \sum_{\lambda=1}^{2} f_\lambda(E) g_\lambda(\theta) + \frac{NZ}{A} r_0 [1+\kappa_{\rm GR}] g_{E1}(\theta), \quad (3)$$

and

$$R^{\rm QD}(E,\theta) = \left[f_{\rm QD}(E) + \frac{NZ}{A} r_0 \kappa_{\rm QD} \right] F_2(q) g_{E1}(\theta), \quad (4)$$

where r_0 is the classical nucleon radius, and the $[1+\kappa_{\rm GR}]$ and $\kappa_{\rm QD}$ terms are enhancements to the GR and QD photoabsorption cross sections expressed in units of the classical dipole sum rule. The QD process describes scattering from correlated proton-neutron pairs and is therefore modulated by the two-body form factor $F_2(q)$, where q is the momentum transferred by the scattered photon. The angular factors are determined from the wave vectors and polarizations of the incident and scattered photons and are listed in Tables I and II.

The real and imaginary components of the forward scattering amplitudes can be obtained using the optical theorem and the Kramers-Kronig dispersion relation [23],

$$\mathrm{Re}\, f_\lambda(E) = \frac{E_\lambda^2 - E^2}{4\pi\hbar c} \frac{1}{\Gamma_\lambda} \frac{\sigma_\lambda E^2 \Gamma_\lambda^2}{\left(E^2 - E_\lambda^2\right)^2 + E^2\Gamma_\lambda^2} \quad (5)$$

and

$$\mathrm{Im}\, f_\lambda(E) = \frac{E}{4\pi\hbar c} \frac{\sigma_\lambda E^2 \Gamma_\lambda^2}{\left(E^2 - E_\lambda^2\right)^2 + E^2\Gamma_\lambda^2}, \quad (6)$$

where E_λ, Γ_λ, and σ_λ are the resonance energy, width, and strength, respectively, and are listed in Table III. As noted

TABLE I. Dipole angular factors.

Λ	$g_\Lambda(\theta)$
$E1$	$\vec{\epsilon}\cdot\vec{\epsilon}'$
$M1$	$(\vec{\epsilon}\times\hat{k})\cdot(\vec{\epsilon}'\times\hat{k}')$

TABLE II. Dipole angular interference factors.

$\Lambda\Lambda'$	$g_\Lambda(\theta)\, g_{\Lambda'}(\theta)$
$E1E1, M1M1$	$(1+\cos^2\theta)/2$
$E1M1$	$\cos\theta$

TABLE III. Lorentzian resonance parameters describing the ^{4}He total photoabsorption cross section. Each resonance is taken to be an $E1$ multipole.

Resonance	$E_{\rm res}$ (MeV)	$\Gamma_{\rm res}$ (MeV)	$\sigma_{\rm res}$ (mb)
1	27.5	16.2	3.06
2	42.8	16.6	0.62
QD	70.0	97	0.20

in Ref. [29], these parameters accurately describe the total photoabsorption cross section data of ^{4}He, which can be treated as containing only electric dipole ($E1$) contributions.

The seagull amplitudes account for nucleon substructure and meson-exchange degrees of freedom and preserve gauge invariance in the total scattering amplitude. The one-body seagull amplitude can be written as

$$R_1^{\rm SG}(E,\theta) = -F_1(q)\left\{\left[Zr_0 - \left(\frac{E}{\hbar c}\right)^2 A\alpha_s\right]g_{E1}(\theta) - \left[\left(\frac{E}{\hbar c}\right)^2 A\beta_s\right]g_{M1}(\theta)\right\}. \quad (7)$$

This process is modulated by the one-body form factor $F_1(q)$, obtained from the Fourier transform of the charge distribution $\rho(r)$,

$$F_1(q) = 4\pi \int \rho(r) e^{i\mathbf{q}\cdot\mathbf{r}} d^3\mathbf{r}, \quad (8)$$

where $\rho(r)$ is a three-parameter Fermi function [30],

$$\rho(r) = \rho_0 \frac{1 + wr^2/c^2}{1 + e^{(r-c)/z}}, \quad (9)$$

with $w = 0.445$, $c = 1.008$ fm, $z = 0.327$ fm, and where ρ_0 has been chosen to satisfy the normalization condition $F_1(0) = 1$.

The two-body seagull amplitude is

$$R_2^{\rm SG}(E,\theta) = -F_2(q)\frac{NZ}{A}(\kappa_{\rm GR} + \kappa_{\rm QD})r_0 g_{E1}(\theta). \quad (10)$$

The two-body form factor is chosen by convention as $F_2(q) = [F_1(q/2)]^2$.

V. RESULTS AND DISCUSSION

The differential cross section, integrated over the full angular acceptance of each detector, is plotted as a function of laboratory scattering angle in Fig. 5(a) and listed in Table IV. Sources of systematic uncertainty include the incident number of photons (±2%), the target thickness (±1%), and the angle-dependent yield extraction. Also shown are unpublished data at $E_\gamma = 60$ MeV measured at the University of Illinois [31], and cross section results from MAX-LAB (Lund) at 87 MeV [29] [Fig. 5(b)]. Our data are consistent with the Illinois measurements [31]. Though the data from Ref. [29] were taken at a higher energy, they are nevertheless useful for comparison with the present data. In this energy regime, the photonuclear response is primarily due to giant resonant effects, as discussed above, so that the scale of the Compton scattering cross section exhibits a modest dependence on beam energy. The higher-energy elastic Compton scattering data from Lund, however, show a notable fore-aft asymmetry absent in the present data, which the authors of Ref. [29] could only account for with an unexpectedly large value of the electromagnetic polarizability of the neutron.

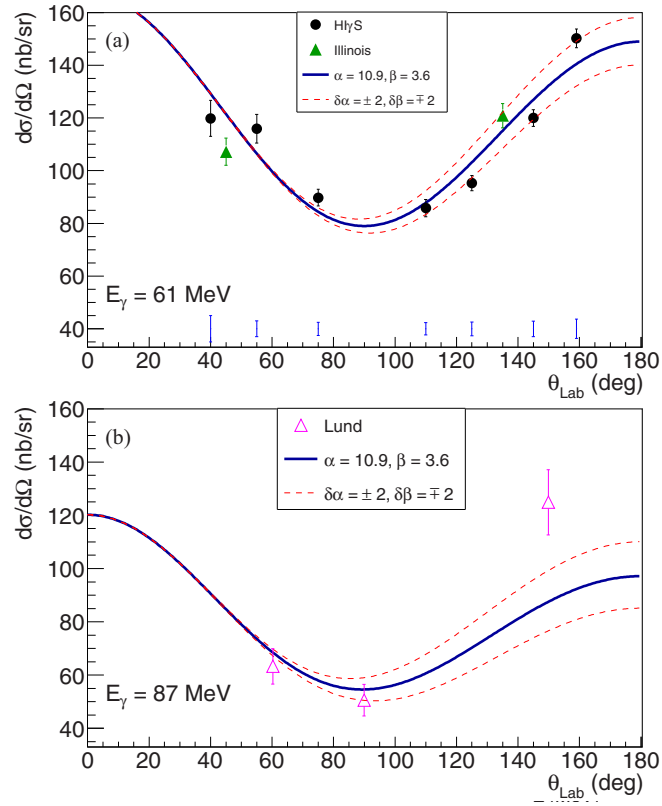

FIG. 5. (a) Differential cross sections measured at HIγS (circles, $E_\gamma = 61$ MeV) and Illinois (triangles, $E_\gamma = 60$ MeV) [31]. The systematic uncertainties for HIγS data are shown in blue underneath each data point. (b) Differential cross section measured at $E_\gamma = 87$ MeV at Lund [29]. The systematic uncertainty was estimated at 15%. The curves were calculated using the phenomenological model described in the text.

TABLE IV. The measured Compton scattering cross section of ^{4}He at $E_\gamma = 61$ MeV shown in Fig. 5(a). The first uncertainty is statistical and the second is the angle-dependent contribution to the systematic uncertainty. The data have an additional overall systematic uncertainty of 2.2%.

$\theta_{\rm Lab}$	$\frac{d\sigma}{d\Omega}$ (nb/sr)
40°	119.8 ± 6.8 ± 4.2
55°	115.9 ± 5.4 ± 1.5
75°	89.8 ± 3.2 ± 1.5
110°	85.8 ± 3.3 ± 1.3
125°	95.3 ± 2.9 ± 1.5
145°	120.0 ± 3.2 ± 1.1
159°	150.2 ± 3.5 ± 1.5

Without a full EFT treatment of these ^{4}He data, the phenomenological model used in this case essentially provides a proof of principle for the utility of a ^{4}He target to determine α_s and β_s. Nevertheless, some significant conclusions can be drawn. In Fig. 5(a), the excellent agreement between the current data and the earlier Illinois data [31] helps confirm the validity of our absolute cross sections. The curves in Fig. 5 were calculated using the phenomenological model with no free parameters. The relevant input parameters for the E1 strength and the QD cross section were taken from fits of ^{4}He photoabsorption [29], and the isospin-averaged nucleon polarizability values α_s and β_s were taken from the EFT values of Eq. (5.8) of the review in Ref. [14]. The resulting phenomenological curve clearly provides a good description of the data at 61 MeV.

The band given by the dotted curves in Fig. 5 illustrates the sensitivity to varying β_s by 2 units, but keeping the sum-rule constraint of $\alpha_s + \beta_s = 14.5$. With fixed $\alpha_s + \beta_s$, the forward-angle cross section remains invariant, so that it is $\alpha_s - \beta_s$ which varies and impacts the back-angle cross section, as seen in Fig. 5. While we have not tried to explicitly fit the phenomenological model to the data, it is apparent that the sensitivity to $\alpha_s - \beta_s$ is larger than the experimental statistical uncertainties of 2–4% in our back-angle measurements. While the forward-angle cross section is not varying, the fact that the phenomenological curve with the sum-rule constraint is fully consistent with our data is a strong confirmation of our analysis procedure and our absolute normalization.

We can extend the comparison to the 87 MeV data of the Lund/Göttingen group [29] as seen in Fig. 5(b). The phenomenological curve for this energy is consistent with the data points at 60° and 90°, but clearly not at 150°. Even the upper dotted curve in Fig. 5(b) does not agree with this back-angle point. To match the curve to the data point at 150°, a much larger value of β_s would be required, far from the currently accepted free-nucleon value. A similar discrepancy with another data set from the Lund/Göttingen group was observed in the case of Compton scattering from ^{16}O [32,33] as compared to data taken at Saskatoon [28].

In summary, a new high-precision data set for Compton scattering on ^{4}He has been measured and shown to be consistent with currently accepted nucleon polarizability values within the framework of a phenomenological model and with existing data at this energy [31]. The higher cross section for the $Z = 2$ nucleus provides enhanced sensitivity to α_s and β_s, and these new data will serve as a motivation for more detailed theoretical treatments to be extended to light nuclei.

ACKNOWLEDGMENTS

The work described in this article is funded in-part by the US Department of Energy under Contracts No. DE-SC0015393, No. DE-SC000536, No. DE-FG02-97ER41033, No. DE-FG02-97ER41041, No. DE-FG02-97ER41, No. DE-FG02-97ER4104, No. DE-FG02-97ER41033, No. DE-SC0016581, No. DE-FG02-03ER41231, and No. DE-SC0016512, National Science Foundation Grants No. NSF-PHY-1714833, No. NSF-PHY-1309130, and No. NSF-1301843, and the Dean's Research Chair program of the Columbian College of Arts and Sciences at The George Washington University. We acknowledge the financial support of the Natural Sciences and Engineering Research Council of Canada. We acknowledge the support of the HIγS operators for the production of the γ-ray beam and the technical staff for support of the experimental setup.

[1] J. A. McGovern, D. R. Phillips, and H. W. Griesshammer, Eur. Phys. J. A **49**, 12 (2013).
[2] C. Patrignani *et al.* (Particle Data Group), Chin. Phys. C **40**, 100001 (2016).
[3] E. Chang, W. Detmold, K. Orginos, A. Parreño, M. J. Savage, B. C. Tiburzi, and S. R. Beane (NPLQCD Collaboration), Phys. Rev. D **92**, 114502 (2015).
[4] M. Lujan, A. Alexandru, W. Freeman, and F. X. Lee, arXiv:1411.0047 (2014).
[5] W. Detmold, B. C. Tiburzi, and A. Walker-Loud, Phys. Rev. D **81**, 054502 (2010).
[6] T. Primer, W. Kamleh, D. Leinweber, and M. Burkardt, Phys. Rev. D **89**, 034508 (2014).
[7] J. M. M. Hall, D. B. Leinweber, and R. D. Young, Phys. Rev. D **89**, 054511 (2014).
[8] M. Engelhardt, PoS: Lattice **2011**, 153 (2011).
[9] M. Engelhardt (LHPC Collaboration), Phys. Rev. D **76**, 114502 (2007).
[10] M. Engelhardt, arXiv:1001.5044 (2010).
[11] J. S. M. Engelhardt and R. Höllwieser (private communication).
[12] W. Freeman, A. Alexandru, M. Lujan, and F. X. Lee, Phys. Rev. D **90**, 054507 (2014).
[13] H. W. Griesshammer, J. A. McGovern, and D. R. Phillips, Eur. Phys. J. A **52**, 139 (2016).
[14] H. W. Griesshammer, J. A. McGovern, D. R. Phillips, and G. Feldman, Prog. Part. Nucl. Phys. **67**, 841 (2012).
[15] F. J. Federspiel, R. A. Eisenstein, M. A. Lucas, B. E. MacGibbon, K. Mellendorf, A. M. Nathan, A. O'Neill, and D. P. Wells, Phys. Rev. Lett. **67**, 1511 (1991).
[16] E. L. Hallin, D. Amendt, J. C. Bergstrom, H. S. Caplan, R. Igarashi, D. M. Skopik, E. C. Booth, D. Delli Carpini, J. P. Miller, F. J. Federspiel, B. E. MacGibbon, and A. M. Nathan, Phys. Rev. C **48**, 1497 (1993).
[17] B. E. MacGibbon, G. Garino, M. A. Lucas, A. M. Nathan, G. Feldman, and B. Dolbilkin, Phys. Rev. C **52**, 2097 (1995).
[18] A. Zieger *et al.*, Phys. Lett. B **278**, 34 (1992).
[19] V. Olmos de León *et al.*, Eur. Phys. J. A **10**, 207 (2001).
[20] L. S. Myers, J. R. M. Annand, J. Brudvik, G. Feldman, K. G. Fissum, H. W. Grießhammer, K. Hansen, S. S. Henshaw, L. Isaksson, R. Jebali, M. A. Kovash, M. Lundin, J. A. McGovern, D. G. Middleton, A. M. Nathan, D. R. Phillips, B. Schröder, and S. C. Stave (COMPTON@MAX-lab Collaboration), Phys. Rev. Lett. **113**, 262506 (2014).

[21] L. S. Myers, M. W. Ahmed, G. Feldman, S. S. Henshaw, M. A. Kovash, J. M. Mueller, and H. R. Weller, Phys. Rev. C **86**, 044614 (2012).
[22] L. S. Myers, M. W. Ahmed, G. Feldman, A. Kafkarkou, D. P. Kendellen, I. Mazumdar, J. M. Mueller, M. H. Sikora, H. R. Weller, and W. R. Zimmerman, Phys. Rev. C **90**, 027603 (2014).
[23] D. H. Wright, P. T. Debevec, L. J. Morford, and A. M. Nathan, Phys. Rev. C **32**, 1174 (1985).
[24] H. R. Weller *et al.*, Prog. Part. Nucl. Phys. **62**, 257 (2009).
[25] R. E. Pywell, O. Mavrichi, W. A. Wurtz, and R. Wilson, Nucl. Instrum. Methods Phys. Res., Sect. A **606**, 517 (2009).
[26] D. P. Kendellen *et al.*, Nucl. Instrum. Methods Phys. Res. Sect. A **840**, 174 (2016).
[27] S. Agostinelli *et al.*, Nucl. Instrum. Methods Phys. Res., Sect. A **506**, 250 (2003).
[28] G. Feldman, K. E. Mellendorf, R. A. Eisenstein, F. J. Federspiel, G. Garino, R. Igarashi, N. R. Kolb, M. A. Lucas, B. E. MacGibbon, W. K. Mize, A. M. Nathan, R. E. Pywell, and D. P. Wells, Phys. Rev. C **54**, R2124(R) (1996).
[29] K. Fuhrberg, D. Häger, T. Glebe *et al.*, Nucl. Phys. A **591**, 1 (1995).
[30] C. W. DeJager, H. D. Vries, and C. D. Vries, At. Data Nucl. Data Tables **14**, 479 (1974).
[31] D. Wells, Ph.D. thesis, University of Illinois at Urbana-Champaign, Champaign, IL, 1990.
[32] D. Häger *et al.*, Nucl. Phys. A **595**, 287 (1995).
[33] M. Ludwig *et al.*, Phys. Lett. B **274**, 275 (1992).